Applied Surface Science 581 (2022) 151763

Contents lists available at ScienceDirect

Applied Surface Science

journal homepage: www.elsevier.com/locate/apsusc

Full Length Article

Rational route to fabrication of uni-dimensional surface gradients presenting stochastic and periodic arrangement of nanoparticles

Hediyeh Malekzad [a,b], Matteo Beggiato [a,b], Dirk Hegemann [c], Sandra Gaiser [c], David Duday [a], Sivashankar Krishnamoorthy [a,*]

[a] MRT Department, Luxembourg Institute of Technology, 41, Rue du Brill, Belvaux L-4422, Luxembourg
[b] Doctoral School in Science and Engineering (DSSE), Faculty of Science, Technology and Medicine (FSTM), University of Luxembourg, Belval, Luxembourg
[c] EMPA, Swiss Federal Laboratories for Materials Science and Technology, Plasma and Coating Group, St. Gallen, Switzerland

ARTICLE INFO

Keywords:
Surface gradient
Nanoparticle self-assembly
Plasma polymer
Block copolymer
Nanofabrication
Adsorption
Quartz crystal microbalance

ABSTRACT

Nanostructure gradients exhibiting graded variation in a nanostructure geometric variable carry high promise as tool for parallel and high-throughput optimization of a range of on-chip devices and functional interfaces. The capabilities to fabricate nanostructure gradients, with desired size and slope, while preserving scalability and operational flexibility is however limited. In this direction, we demonstrate a simple and flexible approach to prepare nanostructure gradients, subjecting a functionalized chip for the adsorption of nanoparticles or ions from aqueous media, with varying durations of exposure along the length of the chip. The configuration is similar to dip-coating, however, with the solution front moving relative to a stationary substrate. The flow rate, dimension of the chamber, and the functional layers are shown as simple handles to achieve the desired gradient morphology. Gradients with stochastic as well as periodic organization of nanoparticle assemblies are demonstrated through the choice of different functional layers underneath the nanoparticle layer, viz. aminosilane monolayers, cross-linked plasma polymer and copolymer templates. The approach paves way to rationally designed gradients, benefitting from the significant flexibility in the choice of operational conditions, without specific constraints on the size of the substrates that can be used.

1. Introduction

Nanoscale devices and interfaces that take advantage of unique optical, electronic and surface behaviour of engineered nanostructures have been leveraged across a range of applications including sensors, data storage, self-cleaning interfaces, energy storage or harvesting, and bio interfaces. In all these cases, the geometric attribute that delivers the optimal functionality is identified by systematic investigations that map the impact of multiple geometry variables and drawing robust correlation between nanostructure and functionality. Given the number of variables, the investigations require numerous experiments to arrive at the most optimal geometries, imposing heavily on the time and resources. In addition, the quality of such outcomes also relies on ensuring identical conditions for all non-variables in the experiment, which requires high degree of reproducibility between the experiments. The task is simplified by resorting to combinatorial approaches that rely on simultaneous and parallel execution of multiple experiments at one time. Prominent examples in this direction includes microarrays that spatially separate the variables into addressable regions, and spatial gradients, that continuously vary a certain variable as a function of distance on a surface. While microarrays allow massively parallel opportunity to investigate parameters, the approaches to produce such arrays serve better to deliver discrete rather than a continuous change in value of the variables under investigation. Spatial gradients on the other hand are better disposed for a graded change in the variable investigated.

Several approaches have been used to produce spatial gradients especially in chemical compositions down to molecular level, typically with gradient dimensions spanning few millimetres. 1-D chemistry gradients of self-assembled monolayers (SAMs) have been fabricated by various techniques, such as dip-coating [1], vapour [2], or gel/liquid diffusion [3,4], printing [5,6], controlled rate infusion [7,8] and electrochemical control [9]. Graded variation in physicochemical parameters such as pH and temperature have shown potential to fabricate surface gradients [7,10,11]. Composition gradients were produced by subjecting mixture of functional amine SAMs with different pKa values

* Corresponding author.
E-mail address: sivashankar.krishnamoorthy@list.lu (S. Krishnamoorthy).

https://doi.org/10.1016/j.apsusc.2021.151763
Received 18 June 2021; Received in revised form 15 October 2021; Accepted 28 October 2021
Available online 1 November 2021

to varying pH [10]. In another study, gradient in density of tethered polymer chains were obtained by using temperature gradients [7]. Similar polymer gradients were fabricated using graded light exposure to result in polymer brushes with control over thickness [12]. Innovative approaches have been explored to generate wide wettability variations based on gradual irradiation-enabled desorption and exchange of functional groups from non-polar methyl containing groups to strongly polar groups and vice versa [13,14]. Besides the mentioned techniques, the large number of literature regarding chemistry gradients are based on utilising plasma-assisted chemical vapour deposition (PCVD) technique [15-18]. Some of the plasma approaches are aimed at modification of the surface of the existing coating to develop a wettability gradient, while other techniques are based on deposition of the desired functional groups with spatial control [16,17]. Plasma-assisted deposition of functional groups for immobilising biomolecules avoid drawbacks of conventional liquid phase surface treatment with aminosilanes, including the environmentally hazardous chemical usage and long preparation time [18]. However, these approaches are particularly well suited to create chemical gradients, they are less suited to produce structural gradients, especially with control over geometries at the nanoscale. Lithography techniques such as photolithography and laser micromachining have been used to produce well-controlled surface gradient patterns with (sub-) micron feature dimensions [19,20]. Non-lithographic approaches such as sandblasting, or nanoparticle adsorption have been used to produce gradients, feature dimensions extending to nanoscale [17,21-27]. Interestingly, most of this work is directed at understanding the impact of nano topography on interaction of biological cells with underlying surface [21,22,24-27].

Nanoparticle gradients are particularly advantageous, as they are well positioned to leverage the advances in the state of the art towards synthesis and adsorption of nanostructures from solution-phase onto solid surfaces [28,29]. The low standard deviations with which nanoparticles can be produced, reduces the spread of geometric variables of features obtained on the gradient. Nanoparticle density gradients have been reported to be obtained using diffusion-limited transport through polymer melts [30], electrostatic self-assembly of negatively charged nanoparticles to positively charged molecular gradients [2,17,31], or via kinetic control over nanoparticle deposition by dip-coating processes [22,23]. Control over kinetic processes provides more flexibility in determining the geometric attributes, viz. the size and slope, of the resulting nanoparticle gradients. However, the kinetic control over nanoparticle density has been achieved only with dip-coating so far. The typical dip-coating set up is open to atmosphere, and suffers from the solvent evaporation, especially for slow dipping speeds. The dimension of the dip-coater determines the size of the sample and the range of displacement, thus being restrictive in process conditions. In all these cases, gradients exhibiting control over nanoparticle size, periodic order or complexity in their organization have not been reported. Further, it is not straightforward to pre-determine the characteristics of the gradients to be produced allowing orthogonal control over the gradient variable. In this direction, we demonstrate a rational approach to fabricate surface gradients that leverage two common time-dependent processes-material adsorption and material growth, in order to deliver nanostructure gradients. The time-dependence of the adsorption process is exploited to systematically vary the nanostructure geometric attributes, namely, nanoparticle size, and surface density of nanoparticles, as a function of distance along the gradient. The processes are further combined with a well-defined and periodic nanoarray template obtained by self-assembly of copolymer colloids. The combination of the surface gradient using pre-defined templates allows exercising orthogonal control over the size and density of nanoparticles obtained. The approach is demonstrated using a simple set up that provide practically unrestricted opportunities in choice of sample size, gradient length and durations of exposure, within a closed, miniaturized environment.

2. Materials and methods

2.1. Materials

Polymers were purchased from polymer source, Inc. (Toronto, Canada). All the substrates, (Silicon wafers and quartz wafers) were obtained from Siegert wafer (Aachen/Germany). The standard AFM tapping mode probes with 330 KHz frequency and 125 μm length were purchased from NanoAndMore GMBH. Quartz Crystal 5 MHz, Gold electrode with Silicon dioxide-coating were obtained from LOT-QuantumDesign GmbH/Germany. Hydrogen tetrachloroaurate(III) trihydrate ($HAuCl_4 \cdot 3H_2O$) (99.9%), (3-Aminopropyl)triethoxysilane (APTES) 99% and sodium citrate dihydrate (~99%) and anhydrous m-Xylene were obtained from Sigma Aldrich (Merck).

2.2. Au nanoparticle synthesis

Gold nanoparticles were synthesized by using Turkevich method [32]. Briefly, 30 mL of 1.02 mM solution of gold chloride was refluxed with 6 mL of 38.80 mM sodium citrate solution for duration of 10 min until appearance of wine red color. The suspension was allowed to cool prior to use.

2.3. Self-assembled silane monolayers

Surface assembled monolayers of (3-aminopropyl)-Trimethoxysilane (APTES), on silicon and glass substrates were obtained by vapour phase deposition. First, substrates were cleaned using plasma etching and by reactive ion etching (Oxford Plasmalab 80, UK), using O_2 plasma (15 mtorr, 100 mW) for a duration of 3 min. The substrates with the activated surfaces were exposed to APTES vapors within a vacuum desiccator under pressure of $\sim 5 \times 10^{-3}$ mTorr for 2 h. Finally, samples were rinsed with isopropyl alcohol and dried with N_2 gun.

2.4. Fabrication of CHN plasma bilayer

Homogenous amino-containing CHN plasma polymer films were fabricated based on the technique developed previously [33]. Fabrication was designed to enhance the stability of amine functionalities of the coating in aqueous media. Accordingly, a vertical gradient consisting of plasma polymers with highly crosslinked base layer and less crosslinked amine functional upper layer was deposited by switching power input and plasma precursor (NH_3/C_2H_4) ratio. The total thickness of the generated bilayer film was approximately 20 nm.

2.5. Experimental set up for nanoparticle gradient fabrication

A pulseless, programmable microfluidic pressure pump (Mitos Pressure Pump, Dolomite, UK) equipped with a flow sensor was used to introduce nanoparticle suspension or the nanoparticle precursor solution into the experimental vessel, where a surface-modified sample (2cmx1cm) was fixed vertically on to the side wall of the vessel along its longer axis. The pump was set to ensure a set flow rate, for the chosen duration of time. The pressure pump can establish stable pressures with the applied pressure range of 0–1 bar and adaptable to employ liquid volumes of μl to litre range depending on the intended application. The gas input can be connected to desired gas source e.g. nitrogen or argon, which helps to assure inertness of atmosphere where necessary. The range of outcomes for the rate of rise as function of the flow rate (from 1 to 100 μL/min) and the vessel radius (1–5 cm) was calculated and plotted as a colour map using functional plot options in origin (Origin Pro 2019, OriginLab Corporation, MA, USA) (Fig. 1c) The nanoparticle densities or dimensions were fitted using Hill isotherm, with the first point taken as (0,0) in all cases.

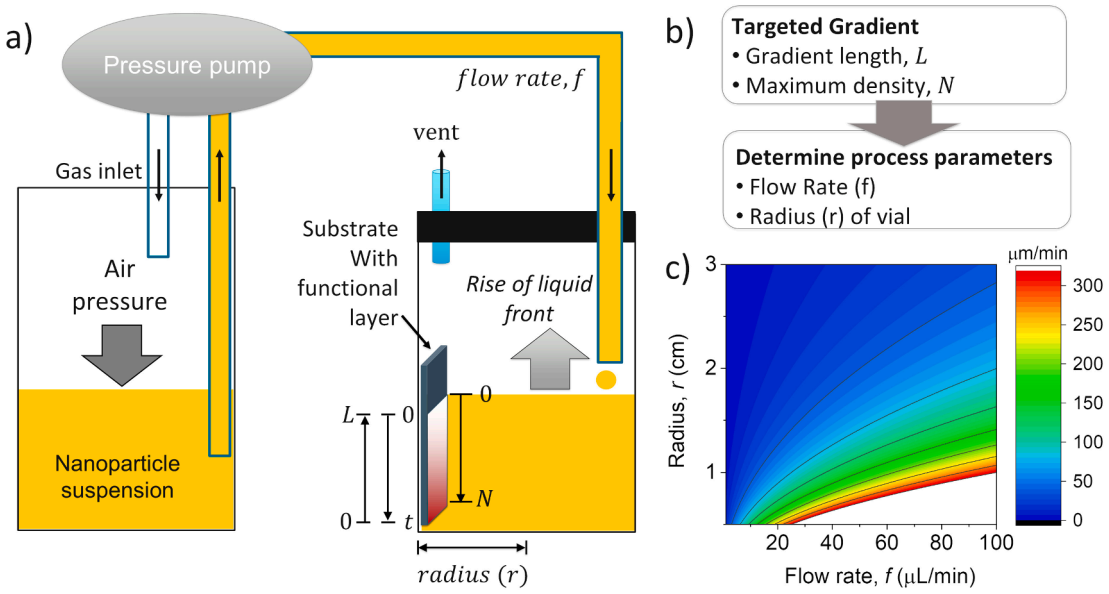

Fig. 1. Schematic illustration of the approach to fabricate nanostructure gradients. (a) The set up used for gradient fabrication. (b) With a targeted length, and maximum density of adsorption, determined by choice of flow rate and the dimension of the vial. (c) Plot showing the dependence of the rate of rise of liquid front as function of the radius of the chamber (r), and flow rate (f).

2.6. Fabrication of micellar templates

Micellar templates were fabricated based on the previously published approach [34]. Polystyrene-block-poly(2-vinylpyridine) (PS-b-PVP) with a molecular weight of 248 kDa for the PS block and 195 kDa for the PVP block were deposited from 0.5 %w/w solutions in m-xylene, on to Si substrates via spin coating at 6000 rpm. The coatings were performed under an environment with controlled humidity. For gold nanoclusters, micellar substrates were further etched by reactive ion etching (RIE) for duration of 30 s to better define patterns to avoid remaining polymers between features. The resulting features were characterized by AFM.

2.7. Quartz crystal microbalance (QCM) measurements

The QCM measurements were carried out using Q-Sense E1 system using a 5 MHz crystal. To measure the nanoparticle adsorption to APTES SAM layers, SiO_2 coated QCM sensors was used. For plasma polymer films and the copolymer films, bare QCM sensors with gold surface were used, as the films of equivalent characteristics can be obtained independent of the surface. The measurements for nanoparticle adsorption was performed in static conditions in a Teflon cell. To measure adsorption of gold precursor, a stable baseline was achieved with a flow of milliQ water, followed by gold chloride solution through a microfluidic cell at a constant flow rate of 10 μL/min throughout the duration of the experiment. The shift in resonance frequency for the 9th overtone was followed, and converted to mass using Sauerbrey's equation. The mass change (Δm) was converted to areal density of nanoparticles (NPs/μm^2) using the equation: $[AuNP] = \Delta m/(V_{NP}\rho_{Au})$, V_{NP} is the estimated volume occupied by a single AuNP with a diameter $d = 11.8$ and ρ_{Au} is the gold density. In general, the applicability of the Sauerbrey's equation lies on the hypothesis that the bound mass does not give rise to any viscoelastic movement, the layer is, thus, rigid and sufficiently thin. If the conditions are not met, it would be possible to incur in an overestimation of the adsorbed mass. To overcome the issue the Δm is considered between two *dry* states of the surface: before injection of the liquid solution and after drying it. The sensor is first equilibrated in air and then the aqueous AuNPs solution is pipetted on the sensor surface. After a given time the sensor is washed with water and the surface is dried. Additionally, the validity of the Sauerbrey's equation to obtain the adsorbed mass, was assured, all throughout, by low dissipation values, which confirm the rigidity of adsorbed layers: $\Delta D/(\Delta f/n) << 0.4{\cdot}10^{-6}$ Hz^{-1} [35].

2.8. Field-Emission scanning electron microscopy (FESEM)

Helios NanoLab™ 650 (FEI, Eindhoven. Netherland) was used to investigate the morphology of the surfaces with an acceleration voltage of 2 kV, a current of 25 pA, and a working distance of 4 mm. No charging was observed for metal particle coated parts, and hence, no additional metal coating was needed. All the prepared gradients were characterized using FESEM by moving few millimetre intervals from the start to the end of the generated gradient height and recording the images. Two magnification values of 100,000× and 200,000× were applied for scanning all the generated surfaces. The images were analysed using ImageJ [36] to obtain the density and the diameter of nanoparticles. The standard deviation of the nanoparticle densities in Figs. 1-4 is indicative of the maximum variability across multiple points corresponding to a specific distance across the gradient.

2.9. Atomic force microscopy (AFM)

AFM analysis was performed with an Innova microscope (Bruker, Santa Barbara) and images were acquired in air in tapping mode at scan rates between 0.5 and 1 Hz. Semi-contact silicon cantilever (RTESP; Bruker) with a spring constant of 40 N/m were employed. Images were processed with the software SPIP (ImageMet) to obtain the height of copolymer templates, and the height of nanoparticles (by precursor adsorption). The standard deviation of nanoparticle dimensions is indicative of the size distribution in diameter and height of nanoparticles. The variability of the dimensions across multiple points corresponding to specific distance across the gradient, yet separated by several millimetres, is lower than the error bars shown for size distributions.

2.10. X-ray photoelectron spectroscopy (XPS)

Elemental characterisation and quantification with XPS were implemented using a Kratos Axis-Ultra DLD instrument equipped with Al Kα source (1486.6 eV), pass energy of 20 eV and an energy resolution

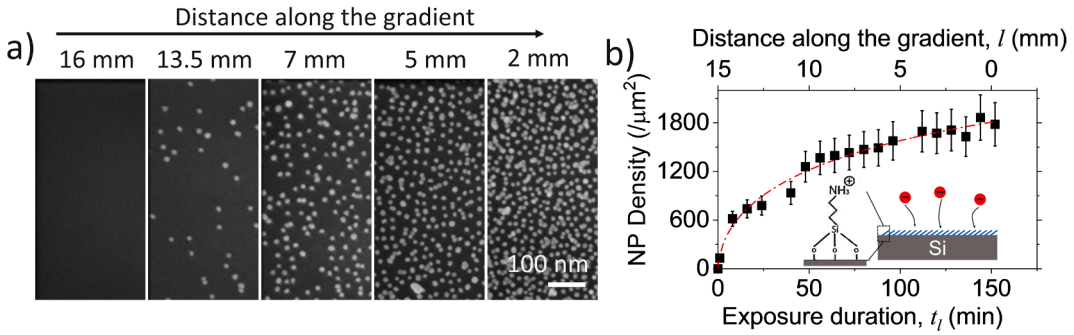

Fig. 2. Unidimensional gradient in gold nanoparticle densities on aminosilane surface (a) FESEM images showing increasing density of gold NP as function of distance along the gradient. (b) Plot of NP density as function of distance (top-X) and corresponding time of adsorption at that distance (bottom-X).

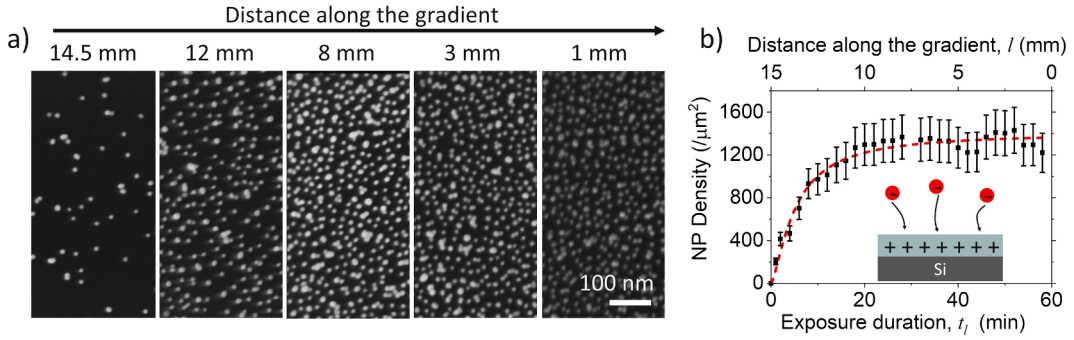

Fig. 3. Unidimensional gradient in gold nanoparticle densities on CHN plasma coated surface (a) FESEM measurements showing increasing NP densities as function of distance along the gradient. (b) Plot NP density as function of distance (top-X) and corresponding time of adsorption at that distance (bottom-X). Dotted line indicates fit to Langmuir-Hill equation.

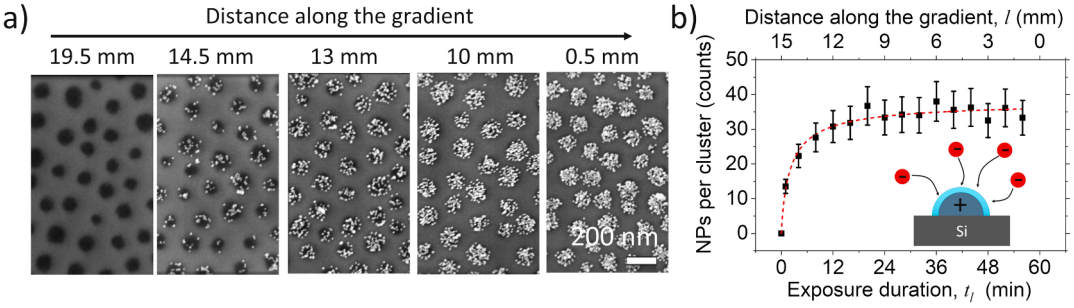

Fig. 4. Unidimensional gradient in cluster size in periodic gold nanoparticle cluster arrays. (a) Top-view SEM measurements as function of distance along the gradient. (b) Plot of nanoparticles per cluster measured from SEM as function of (bottom-X) the duration of exposure to nanoparticle suspension and (top-X) the distance across the gradient. Dotted lines indicate fit to Langmuir-Hill equation.

of 0.5 eV. The survey scans and high-resolution peak scans with 1.5 eV and 0.55 eV energy resolutions were performed to identify and quantify the peaks of interest, respectively. To compensate the charging effect on the sample surface a flooding gun was used to accelerating low energy electrons on the surface. The analysis and data treatment on the resulted spectra were performed using CasaXPS-2315 software. The energy calibration of peaks was performed with respect to C1s main component at 285.0 eV.

3. Results and discussion

3.1. Rationally designed spatial gradients

We present a simplified approach for the fabrication of unidirectional spatial gradients in density and size of metal nanoparticles, relying on time dependent processes of physisorption or chemisorption from aqueous media. The fabrication of the gradient was implemented using a set up as shown in Fig. 1. A chip on which the gradient would be prepared is positioned vertically inside a vial, within which the aqueous suspension of nanoparticles or the precursor solution is gradually increased in volume. The increase in volume translates into increase in the linear distance along the chip exposed to the liquid front. The rate of increase in exposed distance determines the duration of exposure on different points along the length of the chip. The duration of exposure in turn determines the surface density of adsorbate, and thus the nanoparticle densities or the size of the nanoparticles formed. A gradient is thus obtained, with the desired length of the chip, and the maximum duration of exposure set by the user, mainly by controlling the rate of increase of volume, relative to the gradient chip. The volume change can be operationally controlled by both flow rate and the size of the vial (Fig. 1b) providing large flexibility in the choice of the exposure rates, irrespective of the dimension of the sample (Fig. 1c). The configuration further ensures that the chamber remains closed throughout the process, which is particularly helpful to reduce impact of evaporation.

The choice of maximum duration of exposure (t, Fig. 1a) for the gradient chip can be obtained from the kinetics of adsorption as determined by a real-time analysis tool such as surface-plasmon resonance (SPR) or Quartz Crystal Microbalance (QCM). QCM is particularly interesting while measuring adsorption involving plasmonic nanostructures as intended in this report, as optical properties of the adsorbate would not interfere with the mass sensing by QCM. Information of the time to saturation provides help in determining the process parameters, in specific, the rate of increase of length of the chip exposed to the solution. However, due to the difference in configurations, the mass flow of the adsorbate on to the functional layer on the gradient chip (Fig. 1a) is not expected to be the same as encountered in a typical QCM experiment. Nevertheless, the approach can provide reasonably good indication of the time to saturation, which in turn can be a useful parameter to set for the maximum duration of adsorption used for gradient preparation. The resulting gradient would thus represent the equivalent of an adsorption isotherm spanning the length of the chip and representing all adsorbate densities until saturation.

With the targeted length and the maximum exposure duration, one can set rate of exposed length on the gradient chip by controlling the flow rate (f), and the choice of a vessel with an appropriate cross-section (which in our case is cylindrical, with radius r). The design criteria that enables translating the time dependence of the processes as obtained from QCM into spatial dependence of the eventual gradient is obtained as follows: (a) QCM gives an indication of the time (t) to reach the saturated surface density (N) of nanoparticles or precursors. (b) The desired length of the gradient (L), and the time (t) to achieve the surface density N, are used within Eq. (1) to determine rate of increase in height of the solution. Microfluidic pump is then used to set a flow rate, f, that takes into account the cross-section of the cylindrical container with a radius r, to determine the equivalent volume increase necessary for the desired increase in height Eq. (1). The start of the gradient is taken as the point of the chip that is first to contact the solution front. The start of the gradient stays longest within the solution, and thus has the maximum duration of exposure, with progressively shorter durations of exposure along the length of the gradient. The duration of exposure, t_l, of any point at a distance 'l' from the start of the gradient can be expressed as in Eq. (2) and the distance traversed as function of time can be expressed by the Eq. (3).

$$f = \frac{\pi r^2 L}{t} \tag{1}$$

$$t_l = (L - l)^*(t/L) \tag{2}$$

$$l = L - \left(\frac{L}{t}\right)^* t_l \tag{3}$$

The approach is tested to produce well controlled gradients in two different cases, (a) gradients in nanoparticle density exploiting the time dependence of adsorption of gold nanoparticles, and (b) gradients in gold nanoparticle dimensions, exploiting the time dependence in uptake of ionic organometallic precursors. Three different functional layers have been considered to produce the gradients, viz. a) self-assembled monolayers (SAM)s of aminosilane, b) polymer thin films with amine groups deposited using low-pressure plasma, and, c) block copolymer thin films with periodic arrangement of amine containing blocks. The different functional layers carry complementary advantage in the processes used to attain them and carry potential to independently control the outcome of the nanoparticle gradients produced, viz. the density, slope, and periodic arrangement of nanoparticles.

Gold nanoparticle density gradients were prepared relying on random sequential adsorption of negatively charged gold nanoparticles to positively charged functional layers on silicon surface. The positive charges were achieved by three different routes, viz. self-assembled monolayer (SAM) of amine silane, plasma polymer with high concentration of amine groups, and copolymer template containing periodic distribution of amine containing polymeric block. The three choices were compared for the difference in the gradient formation introduced by properties of the functional layer.

3.2. Gold NP gradients on aminosilane SAMs

Amine containing SAMs were prepared on rectangular silicon chips of 2 cm × 1 cm dimensions by exposure to aminopropyltriethoxysilane (APTES) in vapor phase. A preliminary idea of the kinetics of adsorption of gold nanoparticles to the APTES surface was obtained using QCM. QCM sensor chips with silicon oxide coatings were exposed to APTES under identical conditions as used for the silicon chips. In the next step, the adsorption of citrate stabilized gold nanoparticles with a diameter of ~11.8 nm was performed under static conditions to measure the kinetics of adsorption. Based on the time to saturation from the adsorption isotherms, the total time to prepare the gradient was set to 2.5 h (Fig. S1a). The chip with amine SAM was vertically placed in a glass vial with a diameter of 7 mm. Length of the gradient was set to 15 mm. Nanoparticle suspension was introduced into the vial with a flow rate of 15.4 μL / min as determined using Eq. (1). The flow rate was kept constant for the entire duration of the experiment. As discussed earlier, the reference to the start of the gradient (or 0 mm) is taken to be the lower edge of the vertically placed chip that is first contacted by the suspension front (Fig. 1). As the suspension front advances across the length of the chip, the lower edge is exposed to the nanoparticle suspension for the longest duration and consequently exhibits the maximum density of NPs. The highest distance point along the gradient is least exposed to the NP suspension and thus exhibits lower NP densities. The SEM images show clear and systematic increase in nanoparticle densities as function of distance (Fig. 2a). The NP density was determined by image analysis using ImageJ and plotted as function of distance across the gradient (Fig. 2b, top-X), and the corresponding time of exposures (Fig. 2b, bottom-X). The dotted line shows the fit to Langmuir-Hill function (Fig. 2b, Fig. S2a, Supporting Information), used to understand the adsorption as function of time. The nanoparticle densities at the end of 150 min was found to be 1780 NPs/μm^2. The maximum density of nanoparticles can be predicted from random sequential adsorption (RSA) theories. RSA theory predicts the upper limit of adsorbate densities (or the jamming limit) to be achieved at a surface coverage of 54.7% [37]. Taking the size of gold nanoparticles, this coverage would lead to 4938 NPs/μm^2. In relation, the density attained at the maximum duration of exposure is only 33% of the RSA value, or 18% of the surface. The mass changes acquired on the QCM reveal a higher nanoparticle density of 2737 NPs/μm^2, for the same durations, indicating that the impact of the adsorption configurations in the QCM module and the gradient set up, on the nanoparticle densities (Fig. S1a). The lower nanoparticle density in case of the gradient surface could arise from a diffusion limited transport of nanoparticles in the configuration adopted for gradient formation [38].

3.3. Gold NP gradients on plasma polymer films

The gradient formation was repeated with an amine-rich thin film (CHN) obtained by plasma deposition using a technique developed previously [33]. The CHN plasma thin films are designed to enhance the stability of amine functionalities of the coating in aqueous media. Accordingly, a 2 cm × 1 cm silicon chip was coated with plasma polymers with highly crosslinked base layer and less crosslinked amine functional upper layer as we reported earlier [33,39,40]. The total thickness of the generated bilayer film was approximately 20 nm, with a top functional layer of 2 nm and a bottom layer of 18 nm. This bilayer structure allows a limitation of the hydrophobicity recovery through the rotation of the surface chemical groups. The top layer shows N/C ratio of 17.2 at.% (Table S1, Fig. S3, Supporting Information). The CHN layer can be easily deposited on a range of different surfaces. The gradient preparation was performed on the CHN plasma layer with the similar

conditions as for the APTES layers. Based on QCM measurements of the time to saturation for gold nanoparticle adsorption onto the CHN layers coated onto QCM sensors, the time to adsorption was set to 1 h (Fig. S1b, Supporting Information). SEM images reveal systematic increase in nanoparticle density as a function of distance along the gradient (Fig. 3a). The plot of nanoparticle densities as function of exposure durations (or the distance exposed) shows well defined increase with a behaviour as expected of an adsorption isotherm (Fig. 3b, Fig. S2b, Supporting Information). The saturated density of nanoparticles was found to be 1350/μm^2, which represents a surface coverage of 15%. This is similar to the densities observed on APTES layers for a duration of 1 h. The adsorption isotherms AuNP adsorption to CHN layers using QCM for the same duration (Fig. S2b) reveals a density of 1597 NP/μm^2, which is 18% higher than on the gradient samples. The difference between the AuNP densities for the QCM sensor and the gradient for the equivalent exposure durations is lower for the CHN layers as compared to the APTES layers. Unlike APTES layers, the presence of a polymer thin film in case of the CHN layers could potentially enhance adsorption kinetics due to capillary effects.

3.4. Gold nanoparticle cluster arrays with gradients in cluster size

Random sequential adsorption of nanoparticles as in case of APTES and the CHN plasma layers leverage random sequential adsorption resulting in a stochastic arrangement of nanoparticles on surface. We show here that the principle can be readily extended readily to form periodic arrangement of nanoparticles by starting from nanopatterned template exhibiting a periodic variation of electrostatic potential. We had earlier demonstrated the fabrication of periodic arrays of gold nanoparticle clusters through selective electrostatic attachment of citrate-gold nanoparticles to periodic arrays of positively charged copolymer template features [34,41]. The templates are formed out of reverse micelles of polystyrene-block-polyvinylpyridine (PS-b-PVP) copolymer, with the polystyrene corona and polyvinylpyridine core. The pyridine groups in the core acquire a positive charge in aqueous media at pH below its isoelectric point (~8.2) and causes spatially selective immobilization of negatively charged citrate-gold nanoparticles. At maximum coverage, the size of the cluster is determined by the size of the template features. The periodicity of the cluster arrays follows that of the original templates. The templates with a height, diameter and pitch of 34 nm, 83 nm, and 170 nm respectively were obtained from PS-b-PVP with molecular weight of 443 kDa. Rectangular chips with 2 cm × 1 cm containing the copolymer templates were subjected to the gradient formation, with no changes to the size of the gradient, size of the vial and the gold nanoparticle suspension. Based on the adsorption isotherms from QCM (Fig. S1c), the maximum duration of exposure for the gradient was set to 1 h. The SEM images show systematically increasing size of cluster with increasing times of exposure (Fig. 4a). The cluster size, as represented by the number of particles per cluster is plotted as function of the time of exposure and the distance along the gradient (Fig. 4b, Fig. S2c, Supporting Information). The saturation of adsorption of nanoparticles was found to be quicker compared to APTES and CHN layers and can be due to the high density of tertiary amine groups within the core of template features. This is seen to reflect in the AuNP densities of 34 NP/cluster determined from QCM, which is in close agreement with that values observed in case of the gradient for exposure durations of 60 min.

3.5. Gold nanoparticle arrays with gradients in nanoparticle dimensions

In a similar fashion as for fabrication of nanoparticle density gradients, the time dependence of the adsorption of nanoparticle precursors can be used to prepare gradients in the size of nanoparticles. The copolymer template used for formation of NP cluster arrays can be used as template to adsorb negatively charged gold chloride anions by ion-exchange reaction in gold chloride solution. The exchange of negatively charged organometallic precursors within copolymer templates has been shown earlier for in-situ synthesis of inorganic nanoparticles [42,43]. To demonstrate the nanoparticle size gradients, the rectangular chips containing copolymer templates were exposed to rising flow of an aqueous solution of gold chloride. The configuration for gradient preparation was retained, namely, the size of the chip, the vial, and the size of the gradient. The flow rate was set based on Eq. (1) to create the gradient in a duration of 1 h, taking the QCM isotherms into account (Fig. S1d). Following the graded exposure to nanoparticle precursors, the substrate was exposed to O_2 plasma RIE to remove all organic residue. The O_2 plasma RIE exposure has been shown successful in literature as means to produce nanoparticles [44,45]. This results in the inorganic nanoparticles with the dimensions determined by the quantity of gold chloride precursors included within the template (Fig. 5). FESEM measurements show systematic variation in nanoparticle dimensions as function of distance along the length of the gradient (Fig. 5a). The plot of nanoparticle heights as obtained from AFM (Fig. S4), and nanoparticle diameters obtained from FESEM as function of the distance along the gradient length and the duration of exposure shows an increase in nanoparticle height followed by saturation in particle dimensions around an hour (Fig. 5b, Fig. S2d, Supporting Information).

3.6. Nanoparticle gradients – a generic tool to diverse applications

Gradients demonstrated in this work rely on simple adsorption processes, and can be readily extended to produce gradients of other nanoparticles, regardless of the material type, or the substrate used. These gradients are highly promising to optimize nanostructure variables for a broad range of applications that rely on optical and electronic properties of gold nanoparticles. The application of gold nanoparticle assemblies were already demonstrated in our earlier reports and reports published by other research teams, towards plasmon-enhanced spectroscopic sensors [34,46-51], photocatalysis [52,53], charge storage devices [54,55], and bio-interfaces [56,57]. In addition, nanoparticle gradients can be applied to control the surface roughness, through the choice of geometry (e.g. nanoparticles with spike-like features), orientation (e.g. nanorods) and density of nanoparticles. The range of attainable structural gradients can be further extended by using nanoparticles as etch masks in nanolithography processes to produce nanopillars or holes with desired aspect ratios. The approach is far more flexible in the choice of process conditions, as compared to dip-coating, with regards the size of the sample, applicability to curved surfaces and in being less prone to imperfections arising from fluctuations in solvent evaporation (Table S2 in Supporting Information for a comparison). The entire set up is miniaturized and is easily portable and can cater to broad range of gradient size and slopes, without requiring changes to the setup. The study provides a simple, yet flexible and versatile route to periodic as well as stochastic nanoparticle gradients.

4. Conclusions

A rational and flexible approach to fabrication of unidirectional surface gradients presenting graded variation of densities, dimensions and distribution of gold nanoparticles is demonstrated. The approach works by translating the volumetric control over rise of a solution of nanoparticles or its precursors, into linear variation of the durations of contact with a stationary functionalized chip. The approach has potential to deliver a wide range of gradient lengths or slopes, regardless of the chip dimensions, providing flexibility that is well beyond what is commonly achievable using motorized or piezo based dip-coating systems. Drawing a preliminary idea of the kinetics of adsorption using QCM helps in exercising rational choice of operational parameters for gradient formation. The choice of functional layers, viz. aminosilane SAMs, plasma polymer thin films, and copolymer templates, is found to serve as an independent handle to control the nanoparticle densities,

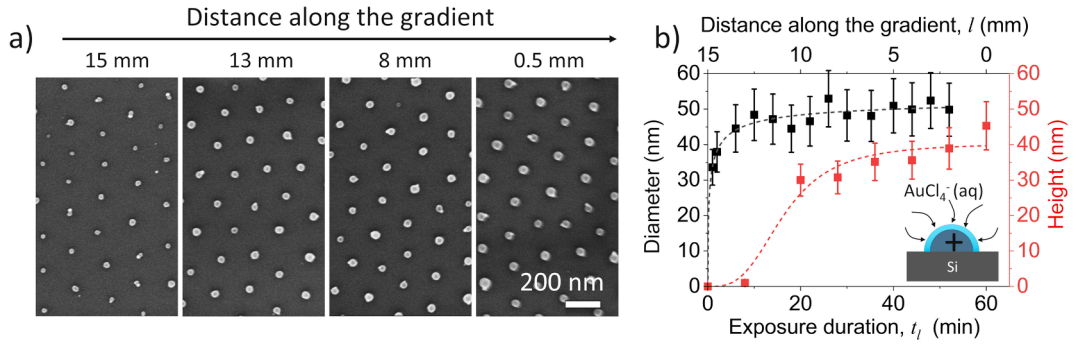

Fig. 5. Unidimensional gradient in nanoparticle size, in periodic gold nanoparticle arrays. (a) SEM measurements show gradient in gold nanoparticle size as function of distance along the gradient. (b) Plot of height (red) and diameter (black) measured from AFM and SEM measurements respectively. Dotted lines indicate fit to Langmuir-Hill equation (For interpretation of the references to color in this figure legend, the reader is referred to the web version of this article.)

while dictating either a stochastic, or periodic arrangement of nanoparticles. Gradients with periodic arrangement of either, nanoparticle clusters exhibiting graded variation in cluster size, or nanoparticles with graded variation in dimensions, was achieved using self-assembled, periodic copolymer templates. The set-up provides benefits of a closed environment that minimizes evaporative or environmental interference during gradient formation, offers a space conserving design, and is easy to implement without the need for sophisticated infrastructure. The approach paves the way to rational design of nanostructure gradients relying on time-dependent surface processes, with possibilities that extend beyond what is shown in the current work.

CRediT authorship contribution statement

Hediyeh Malekzad: Methodology, Writing – original draft, Visualization. **Matteo Beggiato:** Methodology, Writing – original draft, Visualization. **Dirk Hegemann:** Investigation, Writing – review & editing. **Sandra Gaiser:** Investigation, Writing – review & editing. **David Duday:** Methodology, Supervision, Writing – review & editing. **Sivashankar Krishnamoorthy:** Conceptualization, Supervision, Methodology, Visualization, Writing – original draft.

Declaration of Competing Interest

The authors declare that they have no known competing financial interests or personal relationships that could have appeared to influence the work reported in this paper.

Acknowledgements

Funding from Fonds National de la Recherche (FNR) Luxembourg via MASSENA and PLASENS (C15/MS/10459961) projects is gratefully acknowledged.

Appendix A. Supplementary material

Supplementary data to this article can be found online at https://doi.org/10.1016/j.apsusc.2021.151763.

References

[1] L. Li, Y. Zhu, B.o. Li, C. Gao, Fabrication of thermoresponsive polymer gradients for study of cell adhesion and detachment, Langmuir 24 (23) (2008) 13632–13639.
[2] R.R. Bhat, D.A. Fischer, J. Genzer, Fabricating planar nanoparticle assemblies with number density gradients, Langmuir 18 (15) (2002) 5640–5643.
[3] H. Elwing, A. Askendal, I. Lundström, Protein exchange reactions on solid surfaces studied with a wettability gradient method, in: Surf. Forces Surfactant Syst., Springer, 1987, pp. 103–107.
[4] B. Liedberg, P. Tengvall, Molecular gradients of. omega.-substituted alkanethiols on gold: preparation and characterization, Langmuir 11 (1995) 3821–3827.
[5] S.-H. Choi, B.-M. Zhang Newby, Micrometer-scaled gradient surfaces generated using contact printing of octadecyltrichlorosilane, Langmuir 19 (18) (2003) 7427–7435.
[6] T. Kraus, R. Stutz, T.E. Balmer, H. Schmid, L. Malaquin, N.D. Spencer, H. Wolf, Printing chemical gradients, Langmuir 21 (17) (2005) 7796–7804.
[7] L. Ionov, B. Zdyrko, A. Sidorenko, S. Minko, V. Klep, I. Luzinov, M. Stamm, Gradient polymer layers by "grafting to" approach, Macromol. Rapid Commun. 25 (1) (2004) 360–365.
[8] K.M. Ashraf, M.R.K. Khan, D.A. Higgins, M.M. Collinson, pH and surface charge switchability on bifunctional charge gradients, Langmuir 34 (2) (2018) 663–672.
[9] K.M. Balss, B.D. Coleman, C.H. Lansford, R.T. Haasch, P.W. Bohn, Active Spatiotemporal Control of Electrochemical Reactions by Coupling to In− Plane Potential Gradients, J. Phys. Chem. B. 105 (37) (2001) 8970–8978.
[10] L. Tauk, A.P. Schröder, G. Decher, N. Giuseppone, Hierarchical functional gradients of pH-responsive self-assembled monolayers using dynamic covalent chemistry on surfaces, Nat. Chem. 1 (2009) 649.
[11] S. Duhr, D. Braun, Why molecules move along a temperature gradient, Proc. Natl. Acad. Sci. 103 (52) (2006) 19678–19682.
[12] J.E. Poelma, B.P. Fors, G.F. Meyers, J.W. Kramer, C.J. Hawker, Fabrication of complex three-dimensional polymer brush nanostructures through light-mediated living radical polymerization, Angew. Chemie Int. Ed. 52 (27) (2013) 6844–6848.
[13] N. Ballav, A. Shaporenko, A. Terfort, M. Zharnikov, A flexible approach to the fabrication of chemical gradients, Adv. Mater. 19 (7) (2007) 998–1000.
[14] R.R. Fuierer, R.L. Carroll, D.L. Feldheim, C.B. Gorman, Patterning Mesoscale Gradient Structures with Self-Assembled Monolayers and Scanning Tunneling Microscopy Based Replacement Lithography, Adv. Mater. 14 (2) (2002) 154–157.
[15] D.R. Beltrami, J.D. Love, A. Durandet, A. Samoć, C.J. Cogswell, Fabrication and characterization of a planar gradient-index, plasma-enhanced chemical vapor deposition lens, Appl. Opt. 36 (28) (1997) 7143, https://doi.org/10.1364/AO.36.007143.
[16] M. Alexander, T.M. Duc, The chemistry of deposits formed from acrylic acid plasmas, J. Mater. Chem. 8 (4) (1998) 937–943.
[17] R.V. Goreham, R.D. Short, K. Vasilev, Method for the generation of surface-bound nanoparticle density gradients, J. Phys. Chem. C 115 (8) (2011) 3429–3433.
[18] C. Volcke, R.P. Gandhiraman, V. Gubala, J. Raj, T.h. Cummins, G. Fonder, R. I. Nooney, Z. Mekhalif, G. Herzog, S. Daniels, Reactive amine surfaces for biosensor applications, prepared by plasma-enhanced chemical vapour modification of polyolefin materials, Biosens. Bioelectron. 25 (8) (2010) 1875–1880.
[19] J. Wu, J. Miao, Production of centimeter-scale gradient patterns by graded elastomeric tip array, ACS Appl. Mater. Interfaces 7 (12) (2015) 6991–7000.
[20] D. Rajput, S.W. Crowder, L. Hofmeister, L. Costa, H.-J. Sung, W. Hofmeister, Cell interaction study method using novel 3D silica nanoneedle gradient arrays, Colloids Surf. B Biointerfaces 102 (2013) 111–116.
[21] A.B. Faia-Torres, S. Guimond-Lischer, M. Rottmar, M. Charnley, T. Goren, K. Maniura-Weber, N.D. Spencer, R.L. Reis, M. Textor, N.M. Neves, Differential regulation of osteogenic differentiation of stem cells on surface roughness gradients, Biomaterials 35 (33) (2014) 9023–9032.
[22] T.P. Kunzler, C. Huwiler, T. Drobek, J. Vörös, N.D. Spencer, Systematic study of osteoblast response to nanotopography by means of nanoparticle-density gradients, Biomaterials 28 (33) (2007) 5000–5006.
[23] C. Huwiler, T.P. Kunzler, M. Textor, J. Vörös, N.D. Spencer, Functionalizable nanomorphology gradients via colloidal self-assembly, Langmuir 23 (11) (2007) 5929–5935.
[24] T.P. Kunzler, T. Drobek, C.M. Sprecher, M. Schuler, N.D. Spencer, Fabrication of material-independent morphology gradients for high-throughput applications, Appl. Surf. Sci. 253 (4) (2006) 2148–2153.
[25] A.B. Faia-Torres, M. Charnley, T. Goren, S. Guimond-Lischer, M. Rottmar, K. Maniura-Weber, N.D. Spencer, R.L. Reis, M. Textor, N.M. Neves, Osteogenic differentiation of human mesenchymal stem cells in the absence of osteogenic supplements: A surface-roughness gradient study, Acta Biomater. 28 (2015) 64–75.
[26] Q. Zhou, P.T. Kühn, T. Huisman, E. Nieboer, C. Van Zwol, T.G. Van Kooten, P. Van Rijn, Directional nanotopographic gradients: a high-throughput screening platform for cell contact guidance, Sci. Rep. 5 (2015) 16240.

[27] T.P. Kunzler, T. Drobek, M. Schuler, N.D. Spencer, Systematic study of osteoblast and fibroblast response to roughness by means of surface-morphology gradients, Biomaterials 28 (13) (2007) 2175–2182.
[28] M. Grzelczak, J. Vermant, E.M. Furst, L.M. Liz-Marzán, Directed self-assembly of nanoparticles, ACS Nano 4 (7) (2010) 3591–3605.
[29] C. Huang, X. Chen, Z. Xue, T. Wang, Effect of structure: A new insight into nanoparticle assemblies from inanimate to animate, Sci. Adv. 6 (2020) eaba1321.
[30] A. Spinnrock, M. Martens, F. Enders, K. Boldt, H. Cölfen, Controlled Preparation of Nanoparticle Gradient Materials by Diffusion, Nanomaterials 9 (2019) 988.
[31] R.R. Bhat, J. Genzer, B.N. Chaney, H.W. Sugg, A. Liebmann-Vinson, Controlling the assembly of nanoparticles using surface grafted molecular and macromolecular gradients, Nanotechnology 14 (2003) 1145.
[32] J. Turkevich, P.C. Stevenson, J. Hillier, A study of the nucleation and growth processes in the synthesis of colloidal gold, Discuss. Faraday Soc. 11 (1951) 55–75.
[33] J. Dorst, M. Vandenbossche, M. Amberg, L. Bernard, P. Rupper, K.-D. Weltmann, K. Fricke, D. Hegemann, Improving the Stability of Amino-Containing Plasma Polymer Films in Aqueous Environments, Langmuir 33 (40) (2017) 10736–10744, https://doi.org/10.1021/acs.langmuir.7b02135.
[34] F.L. Yap, P. Thoniyot, S. Krishnan, S. Krishnamoorthy, Nanoparticle Cluster Arrays for High-Performance SERS through Directed Self-Assembly on Flat Substrates and on Optical Fibers, ACS Nano 6 (3) (2012) 2056–2070, https://doi.org/10.1021/nn203661n.
[35] I. Reviakine, D. Johannsmann, R.P. Richter, Hearing what you cannot see and visualizing what you hear: Interpreting quartz crystal microbalance data from solvated interfaces, Anal. Chem. 83 (23) (2011) 8838–8848, https://doi.org/10.1021/ac201778h.
[36] M.D. Abràmoff, P.J. Magalhães, S.J. Ram, Image processing with ImageJ, Biophotonics Int. 11 (2004) 36–42.
[37] E.L. Hinrichsen, J. Feder, T. Jøssang, Geometry of random sequential adsorption, J. Stat. Phys. 44 (5-6) (1986) 793–827, https://doi.org/10.1007/BF01011908.
[38] C.-F. Chen, S.-D. Tzeng, M.-H. Lin, S. Gwo, Electrostatic assembly of gold colloidal nanoparticles on organosilane monolayers patterned by microcontact electrochemical conversion, Langmuir 22 (18) (2006) 7819–7824.
[39] M. Vandenbossche, M.-I. Butron Garcia, U. Schütz, P. Rupper, M. Amberg, D. Hegemann, Initial growth of functional plasma polymer nanofilms, Plasma Chem. Plasma Process. 36 (2) (2016) 667–677.
[40] M. Vandenbossche, J. Dorst, M. Amberg, U. Schütz, P. Rupper, M. Heuberger, D. Hegemann, Functionality and chemical stability of plasma polymer films exhibiting a vertical cross-linking gradient in their subsurface, Polym. Degrad. Stab. 156 (2018) 259–268.
[41] V. Suresh, S. Madapusi, S. Krishnamoorthy, Hierarchically built hetero-superstructure arrays with structurally controlled material compositions, ACS Nano 7 (9) (2013) 7513–7523, https://doi.org/10.1021/nn400963a.
[42] X. Li, J. Iocozzia, Y. Chen, S. Zhao, X. Cui, W. Wang, H. Yu, S. Lin, Z. Lin, From precision synthesis of block copolymers to properties and applications of nanoparticles, Angew. Chemie Int. Ed. 57 (8) (2018) 2046–2070.
[43] S. Krishnamoorthy, R. Pugin, C. Hinderling, J. Brugger, H. Heinzelmann, The systematic tunability of nanoparticle dimensions through the controlled loading of surface-deposited diblock copolymer micelles, Nanotechnology. 19 (17) (2008) 175301, https://doi.org/10.1088/0957-4484/19/17/175301.
[44] J.Q. Lu, S.S. Yi, Uniformly sized gold nanoparticles derived from PS-b-P2VP block copolymer templates for the controllable synthesis of Si nanowires, Langmuir 22 (9) (2006) 3951–3954.
[45] R. Glass, M. Arnold, J. Blümmel, A. Küller, M. Möller, J.P. Spatz, Micro-nanostructured interfaces fabricated by the use of inorganic block copolymer micellar monolayers as negative resist for electron-beam lithography, Adv. Funct. Mater. 13 (7) (2003) 569–575.
[46] S. Krishnamoorthy, S. Krishnan, P. Thoniyot, H.Y. Low, Inherently reproducible fabrication of plasmonic nanoparticle arrays for SERS by combining nanoimprint and copolymer lithography, ACS Appl. Mater. Interfaces. 3 (4) (2011) 1033–1040, https://doi.org/10.1021/am1011518.
[47] S. Dinda, F.L. Yap, V. Suresh, R.K. Gupta, D. Das, S. Krishnamoorthy, Quantitative detection with surface enhanced raman scattering (SERS) using self-assembled gold nanoparticle cluster arrays, Aust. J. Chem. 66 (2013) 1034–1038, https://doi.org/10.1071/CH13222.
[48] M. Moronshing, C. Subramaniam, Room temperature, multiphasic detection of explosives, and volatile organic compounds using thermodiffusion driven soret colloids, ACS Sustain. Chem. Eng. 6 (7) (2018) 9470–9479.
[49] S. Yang, X. Dai, B.B. Stogin, T.-S. Wong, Ultrasensitive surface-enhanced Raman scattering detection in common fluids, Proc. Natl. Acad. Sci. 113 (2) (2016) 268–273.
[50] S. Mondal, C. Subramaniam, Xenobiotic Contamination of Water by Plastics and Pesticides Revealed through Real-Time, Ultrasensitive, and Reliable Surface-Enhanced Raman Scattering, ACS Sustain. Chem. Eng. 8 (20) (2020) 7639–7648, https://doi.org/10.1021/acssuschemeng.0c00902.
[51] W.J. Cho, Y. Kim, J.K. Kim, Ultrahigh-Density Array of Silver Nanoclusters for SERS Substrate with High Sensitivity and Excellent Reproducibility, ACS Nano 6 (1) (2012) 249–255, https://doi.org/10.1021/nn2035236.
[52] M.K. Kumar, S. Krishnamoorthy, L.K. Tan, S.Y. Chiam, S. Tripathy, H. Gao, Field effects in plasmonic photocatalyst by precise SiO2 thickness control using atomic layer deposition, ACS Catal. 1 (4) (2011) 300–308, https://doi.org/10.1021/cs100117v.
[53] S. Sarina, E.R. Waclawik, H. Zhu, Photocatalysis on supported gold and silver nanoparticles under ultraviolet and visible light irradiation, Green Chem. 15 (7) (2013) 1814, https://doi.org/10.1039/c3gc40450a.
[54] R.K. Gupta, S. Krishnamoorthy, D.Y. Kusuma, P.S. Lee, M.P. Srinivasan, Enhancing charge-storage capacity of non-volatile memory devices using template-directed assembly of gold nanoparticles, Nanoscale 4 (2012) 2296–2300, https://doi.org/10.1039/c2nr12134d.
[55] V. Suresh, D.Y. Kusuma, P.S. Lee, F.L. Yap, M.P. Srinivasan, S. Krishnamoorthy, Hierarchically built gold nanoparticle supercluster arrays as charge storage centers for enhancing the performance of flash memory devices, ACS Appl. Mater. Interfaces 7 (1) (2015) 279–286, https://doi.org/10.1021/am506174s.
[56] R. Rastogi, M. Beggiato, E.A. Dogbe Foli, R. Vincent, C. Dupont-Gillain, P.-M. Adam, S. Krishnamoorthy, Quantifying Analyte Surface Densities and Their Distribution with Respect to Electromagnetic Hot Spots in Plasmon-Enhanced Spectroscopic Biosensors, J. Phys. Chem. C. 125 (18) (2021) 9866–9874, https://doi.org/10.1021/acs.jpcc.1c00793.
[57] R. Rastogi, E.A. Dogbe Foli, R. Vincent, S. Poovathingal, P.-M. Adam, S. Krishnamoorthy, Hierarchically Structured Plasmonic Nanoparticle Assemblies with Dual-Length Scale Electromagnetic Hot Spots for Enhanced Sensitivity in the Detection of (Bio)Molecular Analytes, J. Phys. Chem. C. 125 (16) (2021) 8647–8655, https://doi.org/10.1021/acs.jpcc.0c10467.